

# Competing fracture modes in brittle materials subject to concentrated cyclic loading in liquid environments: Monoliths

Yu Zhang

*New York University College of Dentistry, New York, New York 10010*

Sanjit Bhowmick and Brian R. Lawn<sup>a)</sup>

*Materials Science and Engineering Laboratory, National Institute of Standards and Technology, Gaithersburg, Maryland 20899-8500*

(Received 9 March 2005; accepted 9 May 2005)

The competition between fracture modes in monolithic brittle materials loaded in cyclic contact in aqueous environments with curved indenters is examined. Three main modes are identified: conventional outer cone cracks, which form outside the maximum contact; inner cone cracks, which form within the contact; and median–radial cracking, which form below the contact. Relations describing short-crack initiation and long-crack propagation stages as a function of number of cycles, based on slow crack growth within the Hertzian field, are presented. Superposed mechanical driving forces—hydraulic pumping in the case of inner cone cracks and quasiplasticity in the case of median–radials—are recognized as critically important modifying elements in the initial and intermediate crack growth. Ultimately, at large numbers of cycles, the cracks enter the far field and tend asymptotically to a simple, common relation for center-loaded pennylike configurations driven by slow crack growth. Crack growth data illustrating each mode are obtained for thick soda-lime glass plates indented with tungsten carbide spheres in cyclic loading in water, for a range of maximum contact loads and sphere radii. Generally in the glass, outer cone cracks form first but are subsequently outgrown in depth as cycling proceeds by inner cones and, especially, radial cracks. The latter two crack types are considered especially dangerous in biomechanical applications (dental crowns, hip replacements) where ceramic layers of finite thickness are used as load-bearing components. The roles of test variables (contact load, sphere radius) and material properties (hardness, modulus, toughness) in determining the relative importance of each fracture mode are discussed.

## I. INTRODUCTION

Many brittle material systems used in biomechanical and other engineering applications are highly susceptible to damage from concentrated surface loading.<sup>1</sup> This is especially true in contact loading with indenting objects, where local stresses can easily exceed the elastic limit and cause fracture. All-ceramic dental crowns and total hip replacements, operating under exacting cyclic loading in hostile aqueous environments, are examples of biomechanical systems that are particularly vulnerable to this kind of damage.<sup>2–7</sup> In the case of a brittle material in contact with curved indenters in single-cycle loading in dry environments, the damage takes the form of a competition between outer cone cracks that initiate outside

the maximum contact from surface flaws and median–radial cracks that initiate from shear-generated microcracks within a quasiplastic damage zone (Fig. 1).<sup>8</sup> Conventional cone cracking is more dominant in harder ceramics, where the contact is mostly elastic; radial cracking is more dominant in softer ceramics, where the contact is more quasiplastic. However, in any given material, either form of fracture can dominate, depending on the loading conditions. Both crack types are accelerated by slow crack growth.<sup>9</sup> Cyclic loading can further accelerate the evolution of median–radial cracks by mechanical fatigue within the quasiplastic zone. In water, cyclic loading can also lead to the generation of a special kind of inner cone crack that forms inside the expanding contact and propagates downward quickly at a relatively steep angle relative to its outer counterpart (Fig. 1).<sup>10</sup> Mechanical fatigue in this case is associated at least in part with hydraulic pumping within the starting cracks.<sup>11</sup>

<sup>a)</sup>Address all correspondence to this author.

e-mail: brian.lawn@nist.gov  
DOI: 10.1557/JMR.2005.0276

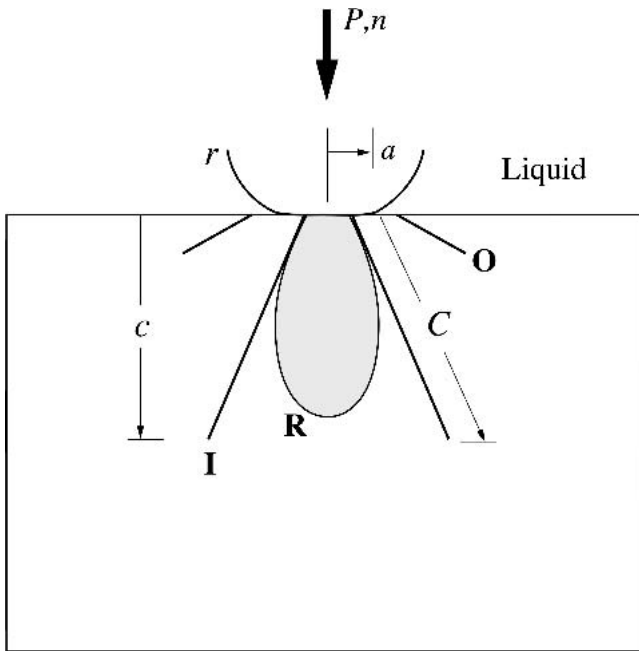


FIG. 1. Schematic illustration of crack geometry for cyclic contact on brittle monolith with sphere of radius  $r$  at load  $P$ , contact radius  $a$ , for number of cycles  $n$  on brittle monolith specimen. Showing three crack modes, depth  $c$ : outer cone cracks (**O**), inner cone cracks (**I**), and median-radial cracks (**R**).

In this study, we examine the competition between the various fracture modes in monolithic brittle specimens, i.e., on specimens sufficiently thick that the loading stresses are concentrated at the top surface. We present crack growth data for thick soda-lime glass slabs indented with tungsten carbide spheres, covering the entire crack evolution from initiation in the near-field to propagation in the far-field. Glass is an ideal model material for this purpose, representative of ceramics at the more brittle end of the spectrum but transparent, enabling in situ observation of each competing fracture mode. However, general conclusions concerning different ceramics can be drawn from the results. Tests are conducted in cyclic loading in water. Fracture mechanics relations derived from a crack velocity equation are used to account for some of the basic trends in the data. We demonstrate that radial cracks and inner cone cracks, even when sluggish in the initiation stages, tend ultimately to outgrow outer cone cracks at large numbers of cycles. Whereas slow crack growth can account for the long-crack propagation of all crack types, superposed mechanical driving forces play a dominant role in the more complex initiation and intermediate stages of the inner cones and radials. The results set the stage for subsequent extension to bilayer structures consisting of brittle layers on compliant support substrates, especially relevant to dental crown and hip replacement structures, where the fractures can lead to catastrophic failure.

## II. ANALYSIS

A complete fracture mechanics analysis of each crack mode under the action of Hertzian contact must ultimately embody both initiation and propagation phases of growth.<sup>1,2</sup> Analysis of the initial small-flaw stages is invariably more complex than the long-crack propagation stages, because of the strong gradients in the near-contact fields. In this section, we summarize some of the basic equations used to describe certain growth phases of the different fracture modes shown in Fig. 1: **O**, outer cone cracks; **I**, inner cone cracks; **R**, radial cracks. A thick specimen is indented with a hard sphere of radius  $r$  at load  $P$  and contact area  $a$  over  $n$  cycles, in a liquid environment. The load  $P(t)$  is taken to be periodic with frequency  $f$ , e.g., sinusoidal or sawtooth (Fig. 2). The ensuing crack depth is  $c$ .

The starting point of any computation of crack evolution is the specification of an appropriate stress-intensity factor of the functional form  $K(P,c)$ . The contact is usually cycled between near-zero and maximum load  $P_m$ . Fractures subject to slow crack growth are governed by a velocity equation<sup>12,13</sup>

$$v = v_0(K/T)^N \quad (1)$$

where  $N$  is an exponent ( $\approx 17$  for soda-lime glass in water<sup>9</sup>),  $v_0$  is a velocity coefficient, and  $T$  is material toughness. In principle, Eq. (1) can be integrated to obtain solutions for the critical number of cycles  $n_1(P_m, r)$  to initiate the cracks and the ensuing propagating crack depths  $c(n, P_m)$ . However, as indicated in Sec. I, superposed mechanical forces can drive the cracks in cyclic loading, especially in liquids, as evidenced for instance by the change in angle between outer and inner cone cracks. Such forces ultimately need to be incorporated into any complete description. However, because of their

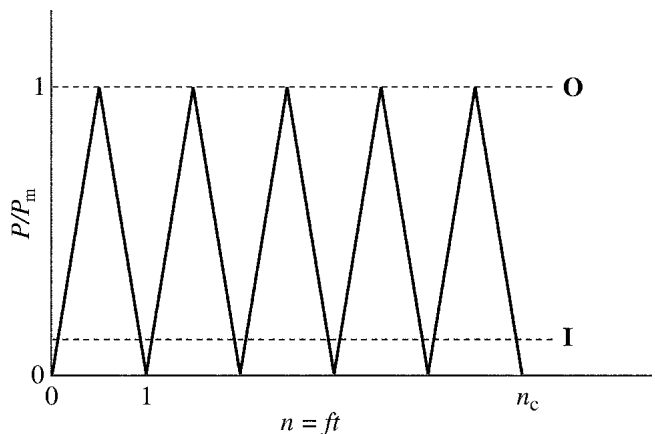


FIG. 2. Fatigue loading  $P(t)$  in cyclic loading, here shown as sawtooth function between zero minimum and maximum at  $P_m$ . Maximum loads at which outer (**O**) and inner (**I**) cone cracks experience tensile stresses at their mouths indicated by horizontal dashed lines.

complexity, only qualitative descriptions of these forces will be presented here.

## A. Initiation

### 1. Cone crack initiation

Consider the growth of a cone crack from a surface location  $R$  (Fig. 1). Such cone cracks initiate from flaws at the contact surface. Outer cone cracks form just outside the maximum contact circle at  $R_O$ , inner cone cracks within the maximum contact circle at  $R_I$ , typically at  $R_I \approx R_O/2$ .<sup>10</sup> The outer cone crack mouths will be subject to a tensile stress  $\sigma_o$  through the entire contact. The inner cone crack mouth will experience negative  $\sigma_o$  during the engulfment stage, inhibiting slow crack growth in the initial stages but enhancing hydraulic pumping of liquid into the confined surface flaws.

Consider for the moment the extension of outer (**O**) cone cracks by slow crack growth alone. The stress-intensity factor takes the functional form  $K(P,c) = \psi\sigma_o C^{1/2}F(C)$ , where  $C$  is the crack length measured along the downward path ( $= c/\sin\phi$ , with  $\phi$  the angle between the cone and the specimen surface),  $F(C)$  is a dimensionless function and  $\psi$  is a geometry coefficient.<sup>9</sup> In the limit of a surface crack under uniform tensile stress  $\sigma = \sigma_o$  in a semi-infinite medium,  $\psi = 1.12$  and  $F = 1$  for all  $C$ . However, in the Hertzian field the tensile stress falls off rapidly along its downward path below the top surface,<sup>14</sup> i.e.,  $\sigma < \sigma_o$  for all  $C > 0$ , so for cone cracks  $F(C) < 1$  at all  $C > 0$ . Hertzian contact relations can then be used to determine a functional dependence  $\sigma_o(P,R,r)$ . Combining this dependence with Eq. (1) then enables derivation of the critical number of cycles to initiate a cone crack from the starting surface flaw. Details of the calculation in terms of the variables of interest here have been given elsewhere<sup>9</sup> and are reproduced in slightly modified form in the Appendix. For outer cone cracks, for which  $\sigma_o > 0$  throughout cycling at  $a \leq R_O$ , the result has the form  $n_I = (P_C/P_m)^{N/2}$  where the quantity  $P_C$  designates the critical load to initiate a cone crack in the first cycle

$$P_C = A[(f/v_0)(rT/E_*)^{2/3}]^{2/N} rT^2/E_* \quad , \quad (2)$$

with  $A = A(N)$  a dimensionless quantity (Appendix). This relation, with its linear  $r$  dependence, is a form of the well-documented Auerbach's law.<sup>2,14</sup> Note the appearance of toughness  $T$  as a dominant material parameter, reflecting an intrinsic resistance to crack extension.

In principle, the same slow crack growth process applies to inner (**I**) cones, with allowance for the fact that the initial surface flaw is exposed to tensile opening stresses only within that portion of the cycle that lies within  $a \leq R_I$ . For  $R_I = R_O/2$  and for the sawtooth loading function in Fig. 2, the same kind of  $n_I(P_m/P_C)$  relation applies but with a substantially higher value of  $A$

in Eq. (2) (see Appendix). The higher number of cycles  $n_I$  to initiate inner relative to outer cone cracks simply reflects a much diminished surface stress level  $\sigma_o$  at the smaller  $R$ . However, the above argument assumes that the governing mechanism of crack extension is slow crack growth. This is surely the case for the outer cone cracks, which remain always outside the oscillating contact.<sup>9</sup> However, inner cone cracks will be driven by a superposed mechanical hydraulic pumping force from intrusion of water into the confined surface fissures at flaw sites during the engulfment stage of contact, incrementally prizing open the surface flaws in successive cycles.<sup>10</sup> Thus the true  $n_I$  will always fall below the predicted value from slow crack growth relations alone. At present, there exists no explicit expression for this additional influence.

### 2. Median–radial crack initiation

In contacts on highly brittle surfaces with blunt indenters median–radial cracks usually form after outer cone cracks and so remain contained subsurface within these preceding cracks. (Exceptions occur beneath sharper indenters—e.g., spheres with smaller  $r$ , Vickers indenters—where the radials break free of any confining cones and spread radially outward.<sup>15</sup>) The evolution of near-surface median cracks is considerably more complex than that for outer cone cracks. Median cracks initiate from coalescence of closed shear microcracks generated within a quasiplastic zone beneath the contact<sup>16,17</sup> and are enhanced in cyclic loading by degradation of friction at the microcrack interfaces.<sup>18,19</sup>

Computation of the critical number of cycles to initiate a crack on a median plane containing the contact axis involves a micromechanical analysis of microcrack coalescence, taking into account the internal frictional degradation.<sup>17</sup> Imposing such a coalescence condition can, in principle, provide a (monotonically diminishing) function  $n_I(P_m/P_Y)$  for the critical number of cycles for median crack initiation,<sup>19</sup> where  $P_Y$  is the load to produce first yield in the contact field<sup>8,20</sup>

$$P_Y = DH(H/E)^2 r^2 \quad , \quad (3)$$

with  $H$  hardness and  $D$  a dimensionless constant. However, only empirical friction degradation functions have been proposed thus far, so functional analytical relations  $n_I(P_m/P_Y)$  are not well established. In this case, hardness is the dominant material parameter—the onset of yield is a necessary precursor to median–radial crack initiation.<sup>16</sup>

Note that, unlike its counterpart for cone cracks in Eq. (2), Eq. (3) does not include provision for slow crack growth (i.e., no  $v_0$  term). Slow crack growth can augment the crack growth, but the mechanical contribution from quasiplasticity remains the dominant factor in initiation.

## B. Propagation

Once the cracks have initiated, they propagate downward through the Hertzian contact zone. The mechanics in the intermediate region are complex for all three crack systems, but especially so for the inner cone and median–radial cracks. The inner cones are especially complex, because of the hydraulic effect. In addition, once they begin to grow downward and outward beyond the contact compression zone and into the surrounding tensile region, the inner cones can undergo additional extension during the contact engulfment stage during cycling. The median–radial cracks are driven by residual stresses within the immediate quasiplastic zone, the intensity of which diminishes because of the cyclic degradation referred to in Sec. II. A. We note only that these additional factors will tend to augment crack propagation within the contact zone, enhancing the fatigue effect.

However, once the cracks enter the tensile far field, i.e., in the long-crack region  $c \gg R$  (Fig. 1), they all tend to the basic geometry of a center-loaded penny crack, with stress-intensity factor

$$K = \chi P_m / c^{3/2}, \quad (4)$$

where  $\chi$  is a dimensionless crack-geometry term. For cone cracks, the quantity  $\chi$  depends on the cone angle; for radial cracks,  $\chi$  depends on the modulus-to-hardness ratio of the indented material.<sup>2</sup> Water can still enter the crack, but any hydraulic pumping tends to die down in this region. Which mode dominates is then decided by the relative values of  $\chi$  for each crack system.

Determination of a crack growth relation in the long-crack region is determined by inserting Eq. (4) into Eq. (1) and integrating. This gives<sup>9</sup>

$$c = c_1 n^{2/3N}, \quad (5)$$

with back-extrapolated crack length intercept at  $n = 1$  defined by

$$c_1 = [(Bv_0/f)^{1/N} (\chi P_m / T)]^{2N/(3N+2)}, \quad (6)$$

where  $B = B(N)$  is another dimensionless quantity.

## III. EXPERIMENTAL

Soda-lime glass plates  $50 \times 25 \times 5.8$  mm were used as monolithic brittle specimens for testing. Side surfaces were polished to enable in situ viewing during loading. Top surfaces were abraded with 600 SiC grit to introduce controlled flaws for cone crack initiation.<sup>21,22</sup>

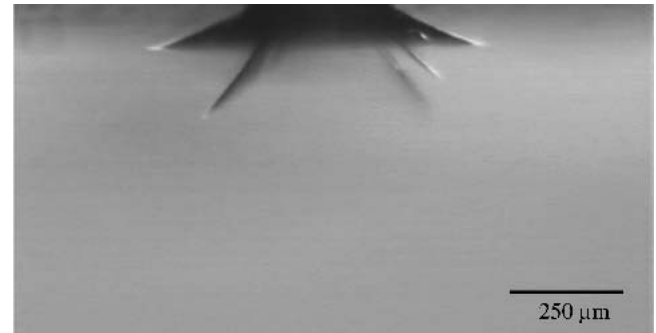
Contact tests were performed with WC spheres of radius  $r = 1.58$  mm for an oscillating load between a small minimum “hold” load  $2 \text{ N}^{10}$  and specified maximum load  $P_m$ , at fixed frequency  $f = 1$  Hz. Some comparative tests were run with spheres of radius  $r = 3.18$  mm and  $5.18$  mm at a maximum load  $P_m = 500$  N. A drop of

water was placed in the contact zone and refreshed throughout the test duration. A video camera was used to view the crack evolution through the glass side walls,<sup>21</sup> slightly tilted upward to view the entire contact zone. The depths  $c$  of each crack system in any given test were thereby measured as a function of number of cycles  $n$  (Fig. 1). In the case of any asymmetrical crack penetration, especially with inner cones, the crack size was measured at the deepest point.<sup>10</sup> Since they tended to form first, the outer cone cracks were most easily tracked. Inner cone and median–radial cracks tended to be obscured by the outer cone cracks in their early stages, making evaluation of critical conditions somewhat subjective in the initiation region. All crack types were clearly visible in the later, fully propagating, stages of growth.

## IV. RESULTS

### A. Crack morphology

Video frames of crack morphologies in their well-developed stages ( $n > 10^4$  cycles) are presented in Fig. 3. Figure 3(a) shows **O** and **I** cone cracks at  $P_m = 120$  N.<sup>10</sup> In this case the inner cones, despite initiating well after



(a)



(b)

FIG. 3. Side views of Hertzian indentation sites in soda-lime glass during cycling at 1 Hz in water with WC spheres of radius  $r = 1.58$  mm after  $n > 10^4$  cycles. (a) Outer and inner cone cracks at  $P_m = 120$  N and (b) dominant median–radial crack at  $P_m = 500$  N. The image in (a) is reproduced from Zhang et al.<sup>10</sup>

their outer counterparts, have propagated deeper. Rotation of the camera about the load axis confirmed a basic axisymmetry of both cone crack types. At the same time, the downward extension of the inner cones was occasionally irregular, with one segment of the crack front sometimes propagating more quickly than the others, subsequently to be overtaken by an adjacent segment.<sup>10</sup>

Figure 3(b) shows a crack pattern at  $P_m = 500$  N. In this case the deepest crack has the median–radial geometry. Note that this **R** crack is confined within the walls of a shallow inner cone, indicating that the median–radial must have initiated last. As mentioned above, the initial stages of median–radial evolution were difficult to trace from the video sequences because of shielding by the preceding cone cracks. The median–plane geometry in this case was readily confirmed by rotating the camera about the contact axis so that the crack was observed edge-on, and by subsequent viewing in transmitted light after completion of the test.<sup>9</sup>

Occasional catastrophic specimen failures occurred after long cycling ( $n > 10^5$ ) at higher loads ( $P_m > 300$  N), from inner cone or median–radial cracks, attesting to the potency of these deep-penetrating crack types.

## B. Crack size data

Figure 4 plots crack depth  $c$  as a function of number of cycles  $n$  for each crack type at one set of loading conditions: fixed sphere radius  $r = 1.58$  mm and maximum load  $P_m = 500$  N. The data points are individual crack measurements, each symbol representing an individual

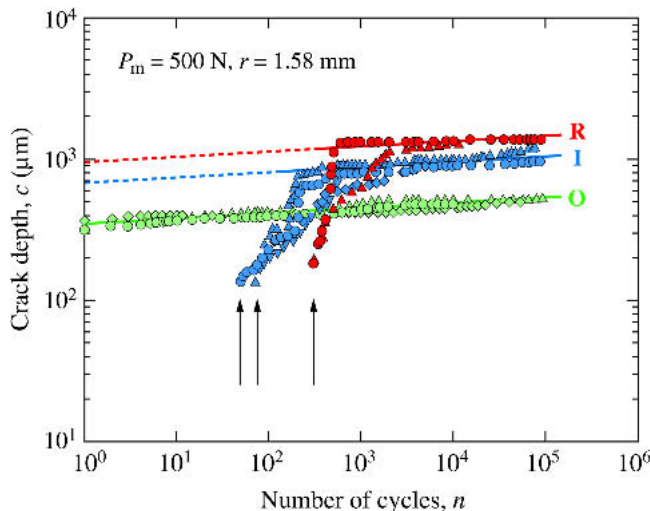


FIG. 4. Crack depth  $c$  as function of number of cycles  $n$  for cracks in surface-abraded glass. Tests at  $P_m = 500$  N with WC sphere of radius  $r = 1.58$  mm, frequency 1 Hz, in water. Data for outer (**O**) and inner (**I**) cone cracks, median–radial cracks (**R**). Inclined lines indicate theoretically predicted asymptotic long-crack response in Eq. (5) for extension solely from slow crack growth, with back-extrapolation to  $n = 1$  (dashed). Arrows indicate crack first sightings. Note how curves for each crack type cross each other.

test. The inclined lines are asymptotic long–crack data fits to a  $c \sim n^{2/3N}$  dependence in Eq. (5), with  $N = 17$  for glass/water. Back-extrapolation of these lines to the left axis at  $n = 1$  enables evaluation of  $c_1$  in Eq. (6) for each crack. Note how the curves cross each other. The outer cones are first to appear, within the first cycle, followed by inner cones at  $n = 50$  to  $70$  cycles and finally median–radials at  $n = 300$  to  $450$  cycles (arrows). Recall that the **I** and **R** cracks are somewhat obscured in the initial stages of the evolution, so that the first data points in this region are “first sightings” and not initiation values. Whereas the outer cones grow steadily downward thereafter, closely following the  $c \sim n^{2/3N}$  relation over most of the data range, the inner cones and especially the radials accelerate strongly after their first appearance and grow much more rapidly in the intermediate region, ultimately growing to greater depths at large  $n$ . Thus, different modes can dominate in different regions of the crack evolution.

Figure 5 plots the measured  $c(n)$  dependence for (a) outer cone, (b) inner cone, and (c) median–radial cracks, for several loads  $P_m$  between 75 and 750 N at fixed  $r = 1.58$  mm. The solid lines representing the  $c \sim n^{2/3N}$  relation in Eq. (5) are included only for the highest load in each case to avoid excessive overlap, but it is apparent that all data sets tend to the same  $n$  dependence in the long-crack region. The data show a systematic shift to smaller long-term crack length  $c$  and to higher number of cycles for first appearance as  $P_m$  diminishes, although the latter shifts are more pronounced in the case of inner cones [Fig. 5(b)] and, especially, radials [Fig. 5(c)].

Analogous  $c(n)$  data are plotted in Fig. 6, but this time for different sphere radii  $r$  at fixed  $P_m = 500$  N. Whereas the data shift to higher  $n$  for first appearance as  $r$  increases, the  $c \sim n^{2/3N}$  asymptote (inclined line) for each crack type is relatively unaffected, confirming that the contact conditions are indeed important in the crack initiation but not in the far-field propagation.

## C. Role of test variables

A comparison between critical numbers of cycles to form the different crack types as a function of maximum contact load  $P_m$  at fixed  $r$  is made in Fig. 7. The data are taken from Figs. 5 and 6, combined with some additional observations at lower loads in which the experiments were terminated after crack formation [i.e., without monitoring the entire  $c(n)$  evolution]. The data for outer cone (**O**) cracks represent pop-in events. These data are somewhat limited because initiation occurs within the first cycle at loads below  $P_m \approx 100$  N. A fit of  $n_1 = (P_C/P_m)^{N/2}$  (Appendix), using  $N = 17$  for glass in water and  $P_C = 100$  N at  $r = 1.58$  mm, is shown as the solid line through the **O** data. The data for the (partially obscured) inner cone (**I**) and radial (**R**) cracks are less well defined, representing first sightings. For the **I** cracks, the

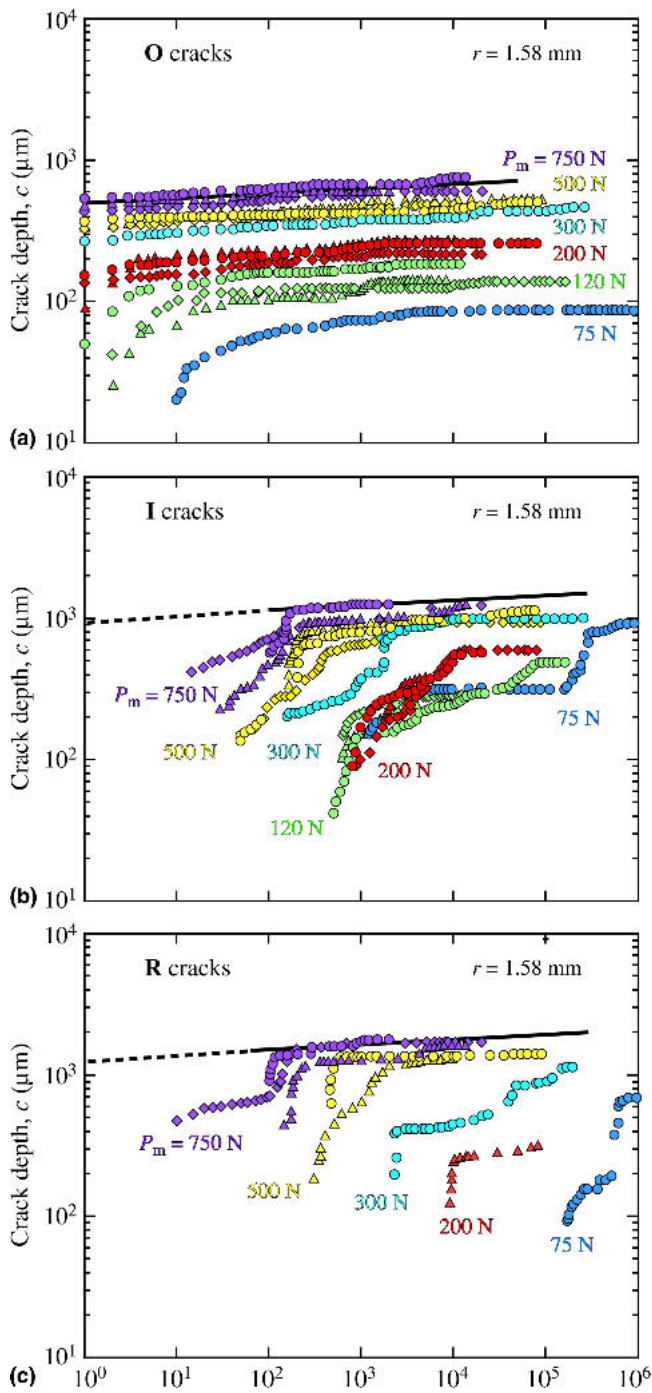


FIG. 5. Crack depth  $c$  as function of number of cycles  $n$  for (a) outer cone cracks, (b) inner cone cracks, and (c) median–radial cracks, in soda-lime glass. Tests in water with WC sphere of radius  $r = 1.58$  mm, frequency 1 Hz, for specified  $P_m$ . Inclined line (shown for highest  $P_m$  only) indicates theoretically predicted asymptotic long-crack function in Eq. 5, with back-extrapolation to  $n = 1$  (dashed).

$c(n)$  data appear to have a stronger dependency than their counterpart **O** cracks. This would appear to confirm the presence of a strong superposed mechanical driving force on the **I** cracks at large number of cycles. Whereas **O** cracks appear to dominate over the bulk of the load

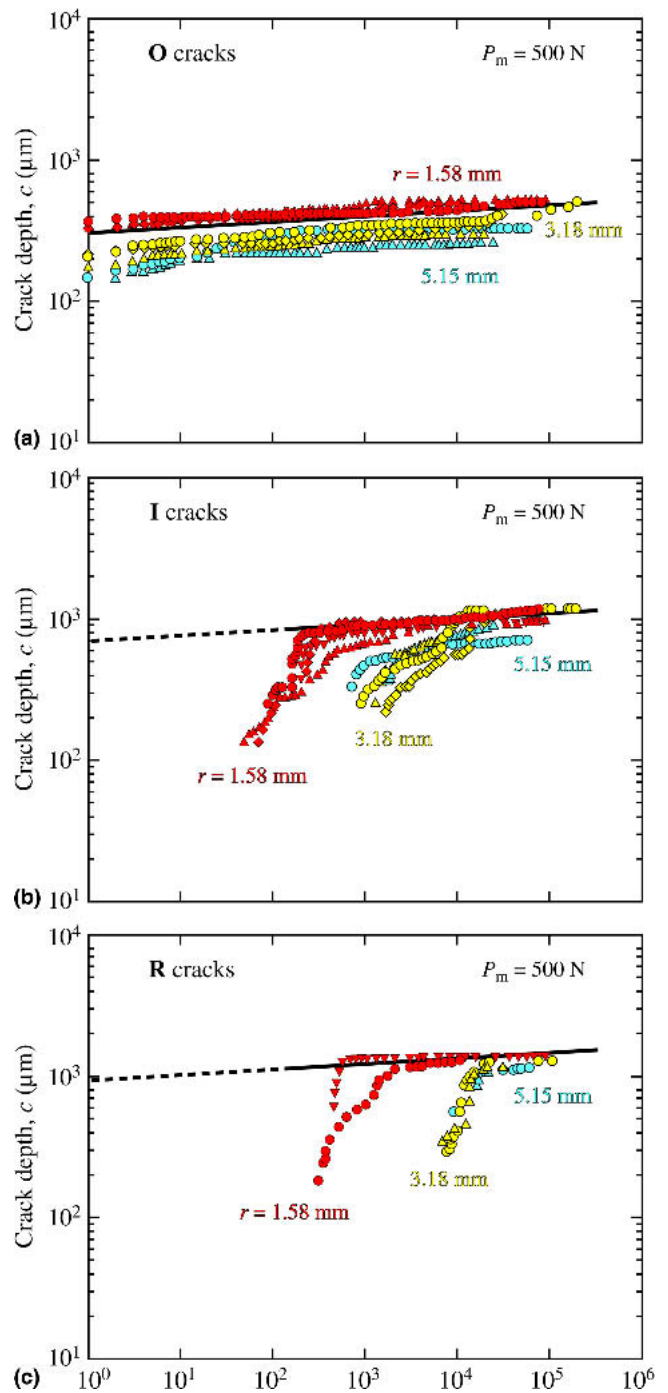


FIG. 6. Crack depth  $c$  as function of number of cycles  $n$  for (a) outer cone cracks, (b) inner cone cracks, and (c) median–radial cracks, in glass. Tests in water with WC spheres at  $P_m = 500$  N, frequency 1 Hz, for specified radii  $r$ . The inclined line (shown for highest  $P_m$  only) indicates theoretically predicted asymptotic long-crack function in Eq. (5), with back-extrapolation to  $n = 1$  (dashed).

range, there is an indication that **I** cracks may actually occur before **O** cracks at low loads ( $P_m < 50$  N) and high number of cycles ( $n > 10^4$ ). Conversely, the indication is that **R** cracks may occur before **I** cracks at high loads ( $P_m > 1000$  N) and low number of cycles ( $n = 1$  to 10).

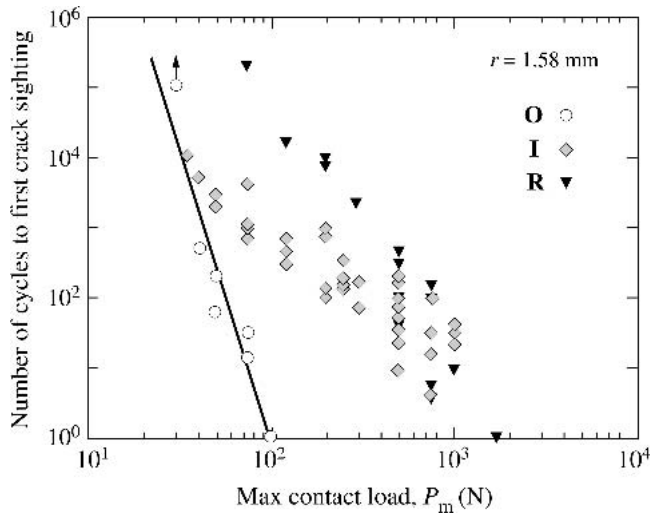


FIG. 7. Plot of number of cycles as function of maximum indentation load  $P_m$  for appearance of outer (O) and inner (I) cone cracks and median-radial cracks (R) in glass/water, fixed  $r = 1.58$  mm. Data for I and R cracks represent crack first sightings, from Figs. 5 and 6. Arrow indicates runout.

Accordingly, the cumulative mechanical effect appears to be less pronounced in the R cracks.

Figure 8 compares behavior in the asymptotic long-crack region, by plotting  $c_1$  back-extrapolated from the data in Figs. 5 and 6 as a function of maximum contact load  $P_m$  for each crack type. The solid lines in this figure represent best fits to  $c_1/P_m^{2/3} = \text{constant}$  in accordance with Eq. (6) at  $N \gg 1$ . These results confirm that R cracks ultimately grow deepest, followed by I then O cracks. The results in Fig. 6 suggest that these conclusions will

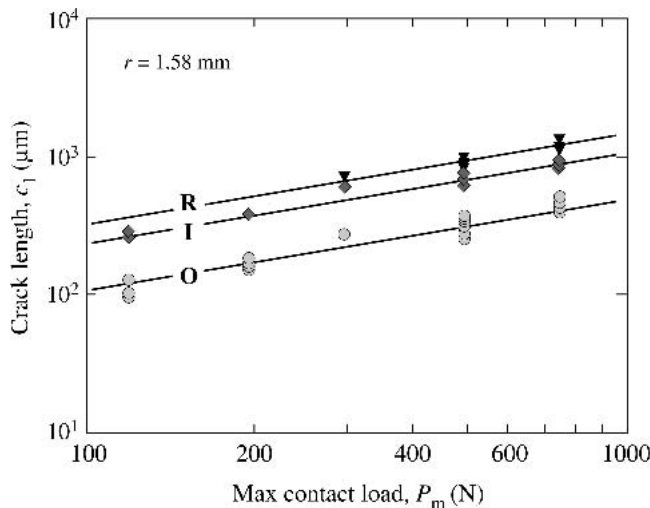


FIG. 8. Plot of  $c_1$  in Eq. (6) as function of indentation load  $P_m$  for outer (O) and inner (I) cone cracks and median-radial cracks (R) in glass/water in long-crack region, fixed  $r = 1.58$  mm. Data obtained by back-extrapolating long-crack data in Figs. 4–6 to the left axis at  $n = 1$ .

be independent of sphere radius  $r$ , consistent with long-crack behavior.

## V. DISCUSSION

The present study has described the competition between different crack modes in brittle materials—outer and inner cone cracks and median-radial cracks—specifically for soda-lime glass in cyclic blunt contact in water. Fatigue in outer cone cracks arises solely from slow crack growth by intrusion of water. Fatigue in inner cone cracks and radial cracks is more complex, driven in large part in their initial stages by superposed mechanical forces arising from hydraulic pumping and precursor quasiplasticity zones, respectively. Whereas in single-cycle contact outer cone cracks form at much lower loads than their competitors, in multi-cycle contact inner cone cracks can occur first (Fig. 7). Median-radial cracks appear to compete with inner cones at high  $P$  and low  $n$ , but are not so competitive in glass at low  $P$  and high  $n$ . Given the relatively innocuous effect of outer cone cracks on subsequent strength response,<sup>2</sup> inner cones and median-radials would appear to pose the major threat to long-term performance in repetitive loading in water, at least in ultra-brittle materials like glass. In coming to this conclusion, it is important to reiterate that whereas radials can form in any environment, inner cones evolve only in cyclic loading in aqueous environments and are therefore less likely to be a factor in air. Once they have penetrated beyond the immediate Hertzian field, radial cracks begin to dominate, followed by inner then outer cones (Fig. 8). This makes the first of these two crack types especially dangerous, not only because of their deep penetration but also because they tend to lie normal to any subsequent tensile stresses from spurious flexural loading.

The analysis in Sec. II provides some explicit equations for the crack evolution. The most complete analysis is for the outer cone cracks, from integration of a power-law crack velocity equation, in both initiation and propagation stages. Initiation relations are less well defined for inner cone and median-radial cracks because of the superposition of mechanical fatigue terms, and are not developed here. Intermediate fracture evolution between the short-crack initiation and long-crack propagation stages is particularly complex, generally requiring numerical (e.g., finite element) analysis. Experimentally, it is difficult to observe the initiation of inner cones and median-radials because of visual shielding by the preceding outer cones. Hence the data in Fig. 7 represent first sightings rather than true initiation conditions. These first sighting data provide an upper-bound for crack initiation. However, once the cracks enter the far-field region the near-field mechanical driving forces die out, and all crack types are governed by a common asymptotic relation of form  $c \sim n^{2/3N}$  based on the same velocity

equation in combination with a simple penny-crack stress-intensity factor.

Of special interest in the present study is the role of maximum cyclic load  $P_m$  and sphere radius  $r$ , reflected in the basic fracture mechanics relations in Sec. II and in the data of Figs. 4 to 6. Both initiation and propagation stages are sensitive to  $P_m$ —high loads reduce the critical number of cycles to form the crack and increase the ultimate crack depth. Only the initiation and intermediate stages are sensitive to  $r$ , as confirmed in Fig. 6. Basically, smaller  $r$  diminishes the critical loads to initiate both cone cracking [Eq. (2)] and quasiplasticity [Eq. (3)]. The  $r$  dependence is stronger in Eq. (3) (quadratic) relative to Eq. (2) (linear), increasing the prospect of yield, and hence radial cracking, with sharper indenters—i.e., an intrinsic size effect.<sup>8,14</sup> In the long-crack region, the fracture can be approximated by a center-loaded penny geometry, eliminating any  $r$  dependence in Eq. (6).

Our current tests have been conducted on soda-lime glass, a prototypical brittle material. The transparency of this material allows direct observation of each damage mode in situ, enabling determination of the full crack evolution. Such in situ observations are not possible for polycrystalline ceramics. However, there is evidence from post-mortem surface and sectioning examinations to confirm the existence of the same crack types in a wide range of ceramic materials.<sup>9</sup> The relative dominance of cone cracks and yield-driven median–radial cracks in ceramics can be gauged by comparing the critical loads  $P_C$  and  $P_Y$  in Eqs. (2) and (3), via a brittleness index  $P_Y/P_C \propto (H/E)(H/T)^2$  for a given sphere radius  $r$  ( $E$  elastic modulus,  $H$  hardness,  $T$  toughness).<sup>8</sup> Thus, cone cracks tend to be dominant in materials with large  $H/E$  and  $H/T$  (brittle), median–radial cracks more dominant in materials with low  $H/E$  and  $H/T$  (quasiplastic). Many polycrystalline ceramics, especially those with coarser microstructures, tend to fall into the second category—in the tougher ceramics cone cracks can be suppressed altogether.<sup>18,19,23–25</sup> In the more brittle materials, which include porcelains used in dental crowns and fine-grain ceramics used in total hip replacements, the material is more susceptible to cone cracking, especially in aqueous environments where inner cones are favored.<sup>9</sup> These inner cone cracks need further study to determine the critical material variables in the fracture mechanics, especially in the first stages of evolution.

Thus we conclude that several fracture modes may compete in brittle materials. A mode that dominates under any given set of conditions may be superseded under a different set of conditions: load level (high or low), load type (static or cyclic), environment (dry or wet), sphere radius (blunt or sharp), and material type (hard or soft). Inner cones and radials are particularly dangerous because they can most easily penetrate even thick brittle layers and thereby lead to catastrophic failure.

## ACKNOWLEDGMENTS

This work was supported by a grant from the National Institute of Dental and Craniofacial Research (PO1 DE10976). Extensive discussions with Herzl Chai are gratefully acknowledged.

## REFERENCES

1. B.R. Lawn and T.R. Wilshaw: Indentation fracture: Principles and applications. *J. Mater. Sci.* **10**, 1049 (1975).
2. B.R. Lawn: Indentation of ceramics with spheres: A century after Hertz. *J. Am. Ceram. Soc.* **81**, 1977 (1998).
3. J.R. Kelly: Clinically relevant approach to failure testing of all-ceramic restorations. *J. Prosthet. Dent.* **81**, 652 (1999).
4. G. Willmann: Ceramic femoral heads for total hip arthroplasty. *Adv. Eng. Mater.* **2**, 114 (2000).
5. G. Willmann: Improving bearing surfaces of artificial joints. *Adv. Eng. Mater.* **3**, 135 (2001).
6. B.R. Lawn: Ceramic-based layer structures for biomechanical applications. *Curr. Opin. Solid State Mater. Sci.* **6**, 229 (2002).
7. B.R. Lawn, A. Pajares, Y. Zhang, Y. Deng, M. Polack, I.K. Lloyd, E.D. Rekow, and V.P. Thompson: Materials design in the performance of all-ceramic crowns. *Biomaterials* **25**, 2885 (2004).
8. Y-W. Rhee, H-W. Kim, Y. Deng, and B.R. Lawn: Brittle fracture versus quasiplasticity in ceramics: A simple predictive index. *J. Am. Ceram. Soc.* **84**, 561 (2001).
9. D.K. Kim, Y-G. Jung, I.M. Peterson, and B.R. Lawn: Cyclic fatigue of intrinsically brittle ceramics in contact with spheres. *Acta Mater.* **47**, 4711 (1999).
10. Y. Zhang, J-K. Kwang, and B.R. Lawn: Deep penetrating conical cracks in brittle layers from hydraulic cyclic contact. *J. Biomed. Mater. Res.* **73B**, 186 (2005).
11. A.F. Bower: The influence of crack face friction and trapped fluid on surface initiated rolling contact fatigue cracks. *J. Tribol.* **110**, 704 (1988).
12. S.M. Wiederhorn and L.H. Bolz: Stress corrosion and static fatigue of glass. *J. Am. Ceram. Soc.* **53**, 543 (1970).
13. S.M. Wiederhorn: A chemical interpretation of static fatigue. *J. Am. Ceram. Soc.* **55**, 81 (1972).
14. F.C. Frank and B.R. Lawn: On the theory of Hertzian fracture. *Proc. R. Soc. London* **A299**, 291 (1967).
15. B.R. Lawn, A.G. Evans, and D.B. Marshall: Elastic/plastic indentation damage in ceramics: The median/radial crack system. *J. Am. Ceram. Soc.* **63**, 574 (1980).
16. B.R. Lawn, N.P. Padture, H. Cai, and F. Guiberteau: Making ceramics 'ductile'. *Science* **263**, 1114 (1994).
17. B.R. Lawn, S.K. Lee, I.M. Peterson, and S. Wuttiphon: Model of strength degradation from Hertzian contact damage in tough ceramics. *J. Am. Ceram. Soc.* **81**, 1509 (1998).
18. N.P. Padture and B.R. Lawn: Contact fatigue of a silicon carbide with a heterogeneous grain structure. *J. Am. Ceram. Soc.* **78**, 1431 (1995).
19. K.S. Lee, Y-G. Jung, I.M. Peterson, B.R. Lawn, D.K. Kim, and S.K. Lee: Model for cyclic fatigue of quasiplastic ceramics in contact with spheres. *J. Am. Ceram. Soc.* **83**, 2255 (2000).
20. R. Mougnot and D. Maugis: Fracture indentation beneath flat and spherical punches. *J. Mater. Sci.* **20**, 4354 (1985).

21. H. Chai, B.R. Lawn, and S. Wuttiphon: Fracture modes in brittle coatings with large interlayer modulus mismatch. *J. Mater. Res.* **14**, 3805 (1999).
22. B.R. Lawn, Y. Deng, and V.P. Thompson: Use of contact testing in the characterization and design of all-ceramic crown-like layer structures: A review. *J. Prosthet. Dent.* **86**, 495 (2001).
23. F. Guiberteau, N.P. Padture, and B.R. Lawn: Effect of grain size on Hertzian contact in alumina. *J. Am. Ceram. Soc.* **77**, 1825 (1994).
24. H. Cai, M.A.S. Kalceff, B.M. Hooks, B.R. Lawn, and K. Chyung: Cyclic fatigue of a mica-containing glass-ceramic at Hertzian contacts. *J. Mater. Res.* **9**, 2654 (1994).
25. S.K. Lee and B.R. Lawn: Contact fatigue in silicon nitride. *J. Am. Ceram. Soc.* **82**, 1281 (1999).
26. S. Timoshenko and J.N. Goodier: *Theory of Elasticity* (McGraw-Hill, New York, 1951).
27. B.R. Lawn: Hertzian fracture in single crystals with the diamond structure. *J. Appl. Phys.* **39**, 4828 (1968).
28. A.G. Evans and E.R. Fuller: Crack propagation in ceramic materials under cyclic loading conditions. *Metall. Trans.* **5**, 27 (1974).

### APPENDIX: CONE CRACK INITIATION

A detailed determination of the critical load to initiate a cone crack subject solely to slow crack growth has been made elsewhere,<sup>9</sup> and essential details are recounted here with some minor modifications to suit the present conditions. The contact radius  $a$  for indentation with a sphere of radius  $r$  at load  $P$  (Fig. 1) for a material of Poisson's ratio  $\nu$  is given by

$$a = (Pr/E_*)^{1/3} \quad , \quad (A1a)$$

with effective modulus  $E_* = 4E/\{3[(1 - \nu^2) + (1 - \nu_1^2)E/E_1]\}$ .<sup>2,26,27</sup> The contact radius  $a = R$  at the cone crack rim defines an engulfment load  $P_R$

$$R = (P_R r/E_*)^{1/3} \quad . \quad (A1b)$$

The radial tensile stress  $\sigma_o$  acting at the surface coordinate in the region  $P \leq P_R$  is

$$\sigma_o = \frac{1}{2}(1 - 2\nu)P/\pi R^2 \quad . \quad (A2)$$

In the region  $P \geq P_R$  the stress  $\sigma_o$  becomes negative.

Let the indenter be subject to a periodic contact load  $P(t)$  between zero and  $P_m \geq P_R$  at frequency  $f$ . The stress-intensity factor for a cone crack of characteristic

dimension  $c$  measured along the downward extending path has the generic form

$$K(C) = \sigma(\pi C)^{1/2} F(C) \quad , \quad (A3)$$

with  $C = c/\sin \varphi$  ( $\varphi$  the angle between the cone and the specimen surface) and  $F(C) < 1$  a dimensionless Greens function.<sup>9,27</sup> Combining the crack velocity relation  $v = dC/dt$  from Eq. (1) in the text with Eqs. (A1)–(A3) and integrating yields a critical condition for cycles  $n_I$  to initiate a cone crack<sup>9</sup>

$$\begin{aligned} n_I &= [H(N)/\alpha^N G(N)](fR/v_0(R^{3/2}T/AP_R)^N \\ &= [H(N)/\alpha^N G(N)](f/v_0)(P_R r E_*)^{1/3} (rT^2/P_R E_*)^{N/2} \quad , \end{aligned} \quad (A4)$$

with  $\alpha = (1 - 2\nu)/2\pi^{1/2}$  and the quantities  $G$  and  $H$  dimensionless integrals<sup>28</sup>

$$G(N) = \eta \int_0^1 [P(f)/P_R]^N d(f) \quad , \quad (A5a)$$

$$H(N) = \int_{C_f/R}^{C_F/R} d(C/R)/[(C/R)^{1/2} F(C/R)]^N \quad , \quad (A5b)$$

where  $\eta \leq 1$  is the fraction of a cycle in which the condition  $P \leq P_R \leq P_m$  remains satisfied (i.e., where the crack is subject to an opening force),  $C_f$  is the size of the starting flaw, and  $C_F$  is the final crack size at cone crack pop-in. The quantity  $G$  is constant for a given loading waveform. Strictly,  $H$  depends on  $C_f$  and  $C_F$ , but not strongly because of the stabilizing effect of the diminishing stress field in the cone initiation.<sup>1,14</sup>

For outer cone cracks, we suppose that the contact expands up to the edge of the cone rim at peak loading. (This is an approximation—usually the cone forms a small distance outside the maximum contact.) Write  $P_R = P_O = P_m$ , corresponding to  $R_O = (P_m r/E_*)^{1/3}$  in Eq. (A1b) and  $\eta = 1$  in Eq. (A5a). For the sawtooth load waveform in Fig. 2,  $\eta = 1$  in Eq. (A5a). For inner cone cracks, take the crack location as  $R_I = R_O/2$ , so that  $P_R = P_I = P_O(R_I/R_O)^3 = P_m/8$  in Eq. (A1) and  $\eta = 1/8$  in Eq. (A5a).

## ERRATA

Eqn. A4 should read:

$$\begin{aligned}n_1 &= [H(N)/\alpha^N G(N)](fR/v_0)(R^{3/2}T/P_R)^N \\ &= [H(N)/\alpha^N G(N)](f/v_0)(P_R r/E_*)^{1/3}(rT^2/P_R E_*)^{N/2}\end{aligned}\tag{A4}$$